RESEARCH ON THE MEMBRANE ACTION OF PROFILED STEEL SHEET-CONCRETE COMPOSITE FLOORS IN FIRE

Shenggang Fan [1,*], Wenjun Sun [1], Hongzhao Wei [1] and Meijing Liu [2]

[1] *Key Laboratory of Conrete and Prestressed Concrete Structure of Ministry of Education, School of civil engineering, Southeast University, Nanjing, 210096, China*
[2] *Department of civil engineering, Southeast University Chengxian College, Nanjing, 210088, China*
[*] *(Corresponding author: E-mail:101010393@seu.edu.cn)*

ABSTRACT: Based on the ISO-834 standard fire curve, fire tests on 2 full-scale profiled steel sheet-concrete composite floors were conducted. The behavior and crack developing process of a composite floor in fire was studied. The change laws of the temperature field distribution and the deflection were given. The failure mode and formation mechanism of the membrane action for the profiled steel sheet-concrete composite floors in fire were revealed. Using the finite element software ABAQUS, the numerical simulation and parametric analysis were performed to research the factors that influence on the membrane action of a composite floor in fire. The results show that the length-to-width ratio, the reinforcement strength and the reinforcement ratio are the main influential factors on the membrane action of a composite floor. The length-to-width ratio less than 2.0 is recommended to make full use of the membrane action of a composite floor. Improving the reinforcement strength and reinforcement ratio can contribute to the bearing capacity of the composite floor with the membrane action considered. Finally, the production condition and judging criteria of the membrane action in a composite floor under fire were also proposed.

Keywords: Composite floor; Membrane action; Fire; Temperature field; Bearing capacity

DOI: 10.18057/IJASC.2015.11.4.5

1. INTRODUCTION

Though the design and analysis method of a building structure in room temperature is well-known, frequent fires have made the safety of building structures an unprecedented challenge. The essential behavior of a structure in fire is that the rise of temperature increase and heat transfer result in the decay of material performance. Parts of the members are damaged and cannot support the structure any more, and the balance of the structure system is broken, with internal force redistribution. As the fire spreads from the center, the damage range of structure extends continuously. As a result, the main structure may lose its bearing capacity or collapse in a wide range. Serious casualties, economic loss and bad social influence often result from the fire of a building structure. Consequently, the response and performance of a structure in fire have attracted great attention all over the world and have gradually become a research hotspot in the field of structure fire resistance.

Many studies show that the calculation theories and design methods of profiled steel sheet-concrete composite floors at room temperature are becoming perfect, whereas the calculation theory in fire is incomplete. Especially, the calculation theory and design method of composite floors, which the membrane action is considered, are not common. With the increment of temperature in fire, a large deflection leads to a membrane action in composite floors, and the ultimate bearing capacity of composite floor in fire as calculated by the plastic hinged lines theory is always relatively low. Thus, the membrane action of a composite floor could be considered in fire-resistant design, it will be of great significance for improving the fire resistance performance of the structure.

There are some relevant studies on the fire resistance and the membrane action of profiled steel sheet-concrete composite floors. Chen et al. [1] performed a fire test on 5 pieces of different composite floors, and the behavior of composite floors with the change of temperature was studied. Li et al. [2] worked out the temperature field of composite floors in fire on the basis of heat transfer theory by developing a computer program and using the finite difference method. The relevant parametric analysis was conducted to derive the simplified calculation formula for the temperature field of a composite floor in fire. Lim et al. [3] performed a fire test on 6 slabs simply supported on 4 sides under a standard fire curve and investigated a variety of parameters that influence on the bearing capacity of slab in fire. A numerical simulation is conducted by the FE software SAFIR, and the result has been proven to be reliable by comparing the simulation results with test data. Bailey et al. [4] performed an ultimate strength test on 15 small-size slabs at room temperature. Based on the yield line theory and the principle of mechanical balance, the membrane action theory was verified and the simplified calculation formula of ultimate bearing capacity was also derived. Chen et al. [5] conducted a fire test on 3 simply supported and 4 continuous slabs subjected to the constant load. A simplified calculation method of the support reaction for a continuous slab during the rise of temperature period was proposed, and it proved to be reliable by comparing test data with the calculation results. Li et al. [6-9] performed the experimental research on 4 full-scale profiled steel sheet-concrete composite floors in fire. The membrane action of the slabs in the fire was verified. Using the numerical simulation analysis, the formula of ultimate bearing capacity and the design method of the composite floor, which the membrane action was considered, were proposed. Based on the result of Cardington fire test, Usmani et al. [10-12] used the energy method to derive the formula for ultimate bearing capacity of the composite floor by solving the equilibrium equation and the deformation compatibility equation, combining the existing research result.

Based on an ISO-834 standard fire curve, a fire test on 2 full-scale profiled steel sheet-concrete composite floors was conducted in this paper. The behavior and crack development process of the composite floors in fire were studied. The temperature field distribution in the composite floors was given. The failure mode and the mechanism of the membrane action of a composite floor in fire were revealed. Using the finite element software ABAQUS, a numerical simulation analysis and parametric analysis were conducted to research the temperature field and behavior of a composite floor in fire. The simulation results were proved to be reliable by comparing with the test data. The length-to-width ratio, thickness, concrete strength, reinforcement strength, reinforcement ratio of slab and thickness of concrete cover were investigated and analyzed to study the influence on membrane action of a composite floor in fire. The research results show that the length-to-width ratio, reinforcement strength and reinforcement ratio were the main influential factor. A larger length-to-width ratio, thickness, concrete strength of slab and thickness of concrete cover will not obviously help to develop the membrane action of composite floors. Finally, the production condition and judging criteria of composite floors in fire were also proposed.

2. FORMATION MECHANISM OF MEMBRANE ACTION IN THE COMPOSITE FLOOR UNDER FIRE

According to the existing results of full-scale fire test on the steel frame and fire cases in the practical engineering, the composite floors will not collapse overall when an external load is close to the ultimate bearing capacity in fire. With the increment of temperature in fire, the cracks in the composite floors were continuously developed and the stiffness of slab was gradually decayed. The larger deformation in the composite floor was generated, which causes the membrane action of a composite floor to appear. The membrane action of a composite floor in fire has been proven in the British Cardington fire test and the Taiwan Eastern Science Park fire case.

2.1 Conditions of Membrane Action in the Composite Floor

According to the calculation theory of membrane action at room temperature proposed by Bailey et al. [13-14], the failure mode and membrane action of a composite floor are closely related to the constraint conditions of the slabs.

When the composite floor was subjected to vertical uniform loads and supported on frame beams, as shown in Figure 1(a), the failure mode of a composite floor depends on the ultimate bearing capacity of the supporting beams and slabs. There are two failure modes. Mode 1 suggests that if the ultimate bearing capacity of a composite floor is larger than the supporting beam, a plastic hinge will first appear in the middle of the supporting beam. With the increment of load, a yield line appears at the middle of the composite floor. The slab fails in a fold line mode. The membrane action will not be generated in this failure mode, as shown in Figure 1(b). Mode 2 suggests that if the ultimate bearing capacity of a composite floor is smaller than the supporting beam, the yield line will first appear inside the floor area. With the increment of load, the yield line will be continually increased. When the supporting beams around the slab have a large stiffness and strong constrain ability, the membrane action will be generated in the composite floor, as shown in Figure 1(c).

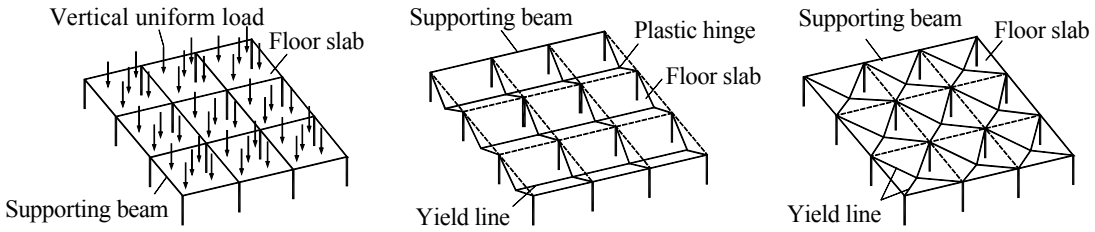

(a) Vertical Load on Floor Slab (b) Failure Mode 1 (c) Failure Mode 2

Figure 1. Failure Mode of Composite Floor

2.2 Mechanism of Membrane Action in the Composite Floor under Fire

The mechanism of the membrane action in the slab under fire is as follows [6, 8]. (1) At the initial stage of the fire, temperature has little influence on the mechanical property of concrete and steel. Compressive stress appears inside the slab because of the thermal expansion result from a high temperature, so the vertical bearing capacity can be improved. (2) As the temperature is increased, the stiffness of slab is decreased, and the material mechanical is property degraded. The concrete at the middle of the bottom slab is cracked, and part of yield line is generated, as shown in Figure 2(a). (3) With the increment of temperature, the yield line is gradually formed with the development of concrete cracks, as shown in Figure 2(b). The failure mechanism is not form until the yield line is appeared as shown in Figure 2(c). However, the floor is not collapse, so the vertical loads can still be subjected. (4) As the temperature gradually rises, the deflection of slab is continually increased, and the compression reinforcement at the top of the floor slab begins to transform to tensile reinforcement. The floor slab membrane action is gradually formed, with cracks appeared in the corner on the top surface of the slab, as shown in Figure 2(d). (5) With the increment of temperature, the membrane action is enhanced, and deflection at the middle of the slab is magnified. The cracks in the corner on the top surface of the slab is increased, and a yield line is appeared on the edge of slab (approximate ellipsoidal), as shown in Figure 2(e). (6) As the development of cracks, the yield line is more and more obvious. Most of the concrete in the ellipsoidal area is cracked, and the vertical loads are mainly subjected by the tensile reinforcement. The floor will be reached the ultimate state, as shown in Figure 2(f).

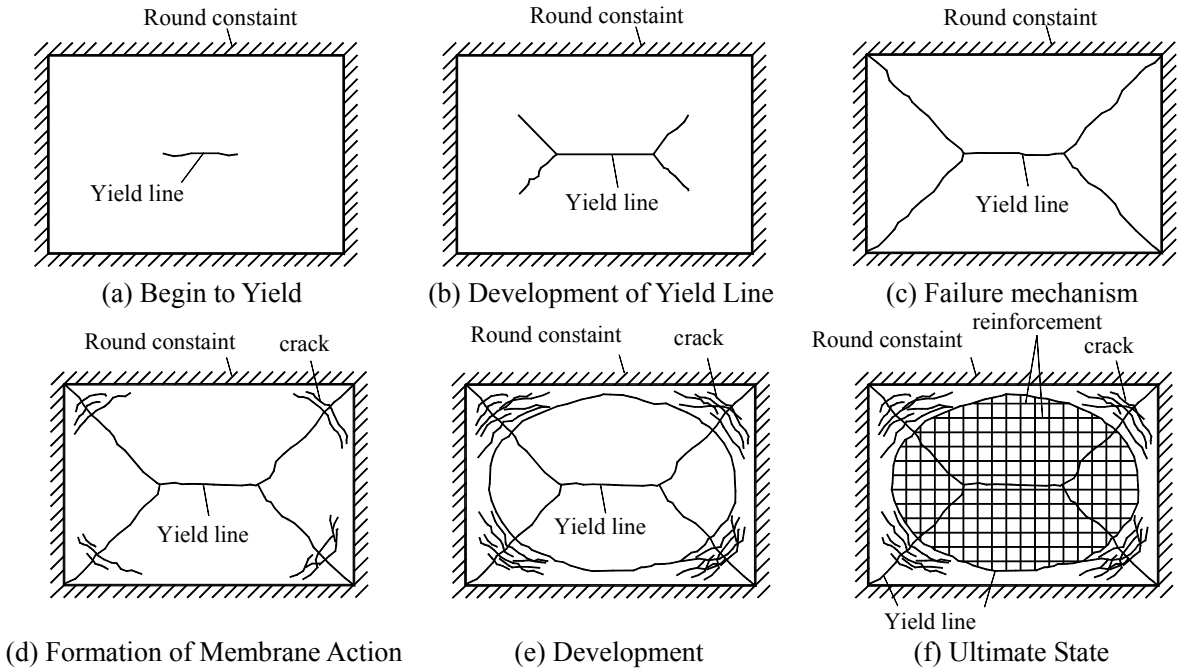

(a) Begin to Yield (b) Development of Yield Line (c) Failure mechanism

(d) Formation of Membrane Action (e) Development (f) Ultimate State

Figure 2. Membrane Action of a composite floor in Fire

3. FIRE TEST OF A COMPOSITE FLOOR

3.1 Test Specimens

Based on an ISO-834 standard fire curve, a fire test on 2 full-scale profiled steel sheet-concrete composite floors was conducted. The size of the composite floors was 3.0 m×1.86 m (length × width), and the thickness was 130 mm. The YX51-253-760 profiled steel sheet was adopted, which was 1 mm thick, and the yield strength of steel was 235 N/mm^2. The concrete strength was 11.9 N/mm^2. Reinforcements were not laid at the bottom of the composite floor, and double two-way reinforcements were laid on the top of the slabs. The diameter of reinforcements was 8 mm and the distance was 150 mm. The strength of reinforcements was 310 N/mm^2. The thickness of the concrete cover was 25 mm. The load ratios (the ratio of the test load and ultimate load at room temperature) of the two composite floors were 0.6 and 0.75 in the test. A detailed size and grouping of the test specimens is shown in Table 1.

According to Bailey's theory [15], the premise of membrane action in fire is the strong constraint conditions of supporting beams around the slabs. After analyzing a variety of supporting beam solutions (such as a steel beam and a concrete beam), the reinforced concrete beam with larger stiffness was arranged around the composite floor. Therefore, the displacement in the horizontal direction of the slab can be constrained under a fire. Based on ABAQUS, the section size was determined by the repeated calculation of the supporting beams. The section sizes of supporting beams were 400 mm×350 mm on the short span and 500 mm×350 mm on the long span. The detailed sizes of test specimens and the surrounding supporting beams are shown in Figure 3.

Table 1. Details Sizes and grouping of Test Specimens

Specimen	Size(length × width) /m	Thickness /mm	Concrete thickness on the top of slab /mm	Reinforcement distribution on the top of slab	Cover thickness /mm	Load ratio
TB-1	3.0×1.86	130	79	φ8@150	25	0.60
TB-2	3.0×1.86	130	79	φ8@150	25	0.75

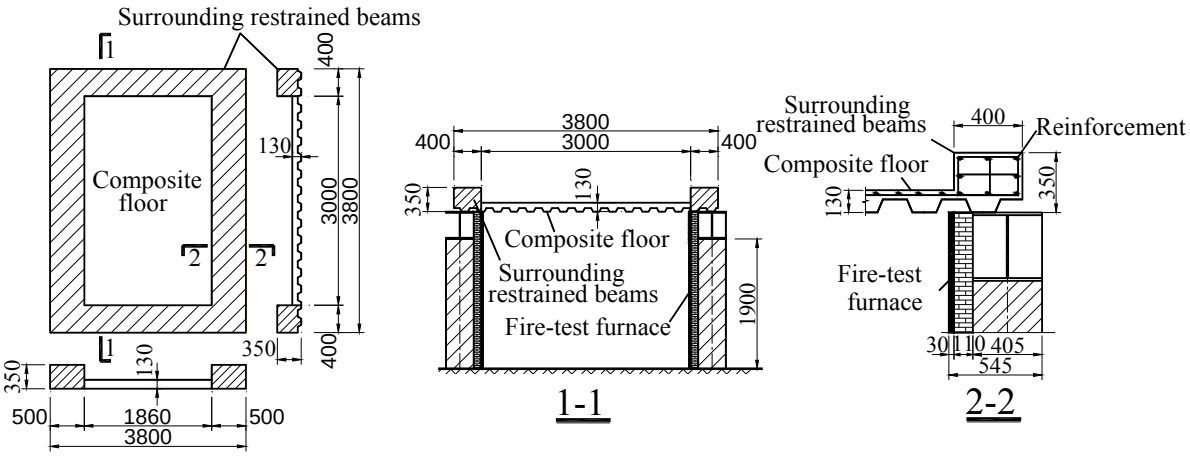

Figure 3. Detail Sizes of Test Specimen and Supporting Beams

To avoid local compression failure at the loading point by a concentrated load, steel plates of 200 mm×200 mm×10 mm were arranged at the loading point on the composite floor, as shown in Figure 4(a). Considering the rotation in the process of slab deformation, a semi-steel ball was in contact with the composite floor, which was placed at the loading end, as shown in Figure 4(b).

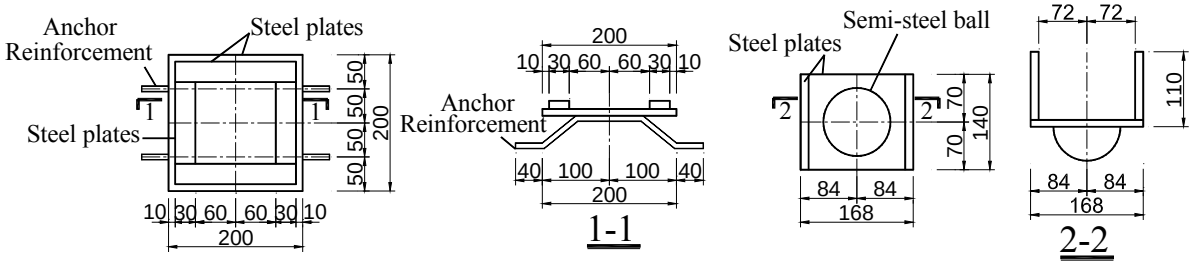

(a) Steel Plate (b) Semi-steel Ball

Figures 4. Size of Steel Plate and Semi-steel Ball at Loading Point

The form work manufacture, reinforcement construction and concrete pouring of the composite floor were completed in the laboratory. The curing time of the concrete was 28 days. The manufacturing process of the test specimens is shown in Figure 5.

(a) Profile Steel Sheet (b) Steel Plate (c) Semi-steel Ball

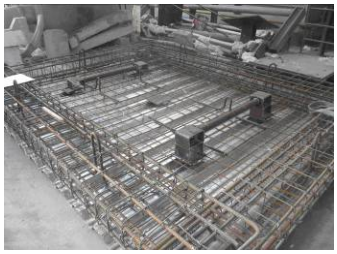
(d) Reinforcement Construction


(e) Concrete Pouring


(f) Specimen

Figure 5. Manufacture Process of test Specimens

3.2 Test Method

The transient method was adopted in the fire test of composite floor in which a specific load was applied on the slab at room temperature, followed by the temperature rising. The failure phenomenon and membrane action of a composite floor in fire could be investigated. In a conventional fire test of the bearing capacity of slab, the test is completed when the deflection of the slab in fire is more than L/20 (L represents the short span of the slab). However, this criterion is not applicable for the fire test on the membrane action of a composite floor, due to the membrane action generated only in the condition of large deflection. The following two conditions were adopted as the end criterions of fire test on the membrane action: (1) fire-resistant time of a composite floor (about 90 min) and (2) overall collapse of a composite floor.

According to the existing results of fire test, the value of load ratio was selected from 0.3 to 0.7 in a transient fire test of a composite floor. To study the membrane action of a composite floor in fire, a larger load ratio is needed. The load ratios of specimen TB-1 and TB-2 are selected respectively 0.6 and 0.75. The ultimate load of the two composite floors is 64.47 N/mm^2, based on the calculation theory of bearing capacity at room temperature. The test loads of TB-1 and TB-2 are 38.68 N/mm^2 and 48.35 N/mm^2, respectively, in accordance with the load ratio.

The point loading method was adopted in the fire test of composite floor, where the vertical uniform load was equivalent to 5 concentrated loads. The slab was divided into 5 areas, as shown in Figure 6(a). Each loading point was located at the centroid of the corresponding bearing area. The concentrate load was applied by a distributive girder and a separate hydraulic jack between point 1 (point3) and points 2 (point4), and applied directly by a separate hydraulic jack at loading point 5, as shown in Figure 6(b). The loading device is shown in Figure 6(c). To avoid the overturn of the distributive girder in the side direction, two steel bracings were set between point 1 (point3) and point2 (point4). In the process of test load, 3 jacks should be worked at the same time to ensure the synchronism of each loading point. The test load value of each loading point can be worked out, as shown in Table 2. A constant amplitude loading was adopted in the fire test, and the load value of each level is shown in Table 2.

The temperature of test furnace was increased according to the ISO834 curve, as shown in Formula (1). The duration time of fire is 90 min.

$$T(t) - T_0 = 345\log_{10}(8t + 1) \tag{1}$$

Where, T(t) represents the air temperature of test furnace when time t; T_0(°C) refers to the room temperature, which is usually 20°C; and t represents the time of the fire.

Table 2. Test Load and Loading Levels of Specimens

Specimen	Loading point	Test load / kN		Loading level / kN				
		Loading point	Jack	Level 1	Level 2	Level 3	Level 4	Level 5
TB-1	1~4	100	200	40	40	40	40	40
	5	56.5	56.5	11.3	11.3	11.3	11.3	11.3
TB-2	1~4	100	200	40	40	40	40	40
	5	56.5	56.5	11.3	11.3	11.3	11.3	11.3

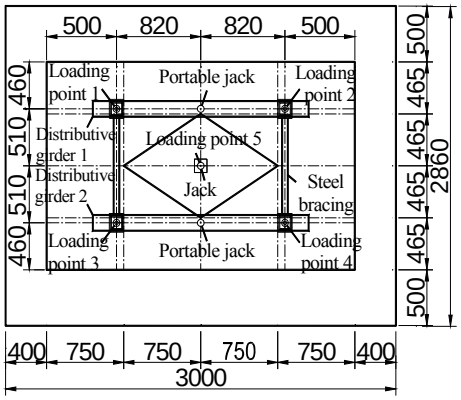

(a) Distribution of Loading Point

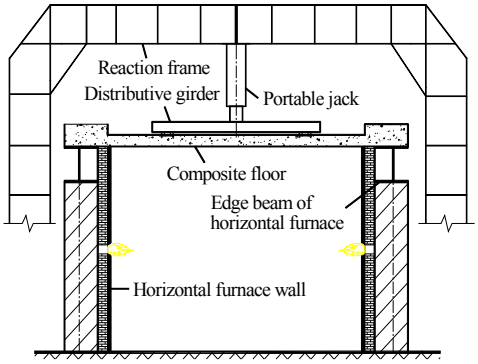

(b) Distributive Girders and Jacks

(c) Loading Device

Figure 6. Loading Point and Loading Device

3.3 Test Device

A horizontal fire furnace was adopted in the fire test of a composite floor, as shown in Figure 7(a). The size of the furnace chamber was 4 m×3 m×1.9 m, and the highest temperature was 1150°C. There were 4 measuring points of temperature in the furnace. The temperature and displacement could be recorded automatically once per minute by the data collection system of the fire furnace. There were four 50-ton reaction frames on the horizontal fire furnace that could move horizontally according to the demand. Two separate hydraulic jacks and an oil jack of 50 t were used in the test, as shown in Figures 7(b) and (c).

(a) Horizontal Fire Furnace (b) Separate Hydraulic Jack (c) Oil Jack

Figure 7. Test Device

A cable displacement meter was used to measure the deflection of the slab, as shown in Figure 8 (a). K-thermocouple (0.5 mm in diameter) was used to measure the temperature of slab, as shown in Figure 8(b). The measuring range of the thermocouple was 0~1300°C. To ensure the accuracy of the data, the thermocouple was wrapped with a ceramic tube. During the first period of fire test (when the temperature is lower), the strain of reinforcement was recorded by a data acquisition instrument, as shown in Figure 8(c).

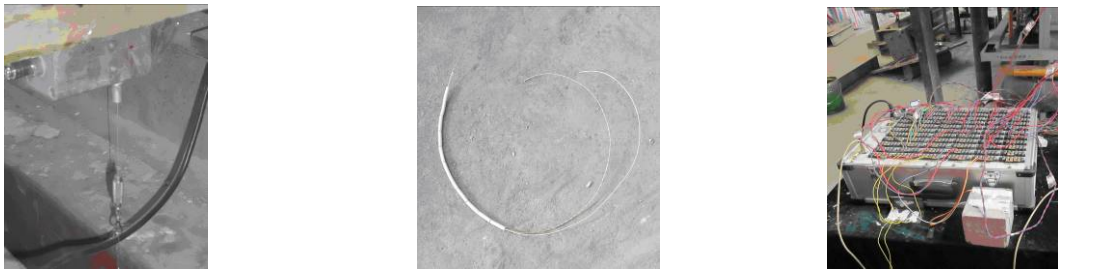

(a) Displacement meter (b) Thermocouple (c) Strain Acquisition Instrument

Figure 8. Data Acquisition Equipment

3.4 Arrangement of Measuring Point

The content of the measurement in the fire test mainly included the temperature and the deflection of slab. The thermocouples were arranged inside the slab before the concrete was poured. The measuring point distribution of temperature for reinforcement and slab are shown in Figures 9(a) and (b). The measuring point distribution of deflection is shown in Figure 9 (c).

3.5 Test Process and Failure Phenomenon

The two phases were included in the process of fire test, which were loading at room temperature and the rise of temperature. Because the specimen TB-1 was similar to TB-2, the failure process and failure phenomenon of TB-2 in fire are only introduced.

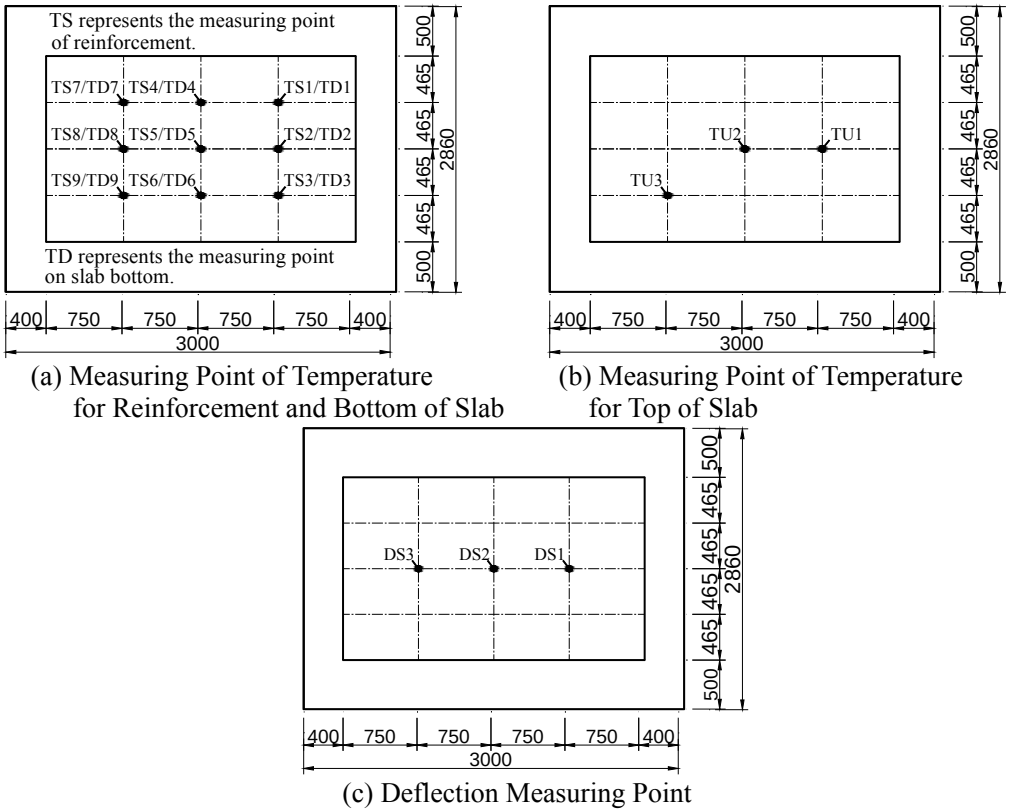

(a) Measuring Point of Temperature for Reinforcement and Bottom of Slab

(b) Measuring Point of Temperature for Top of Slab

(c) Deflection Measuring Point

Figure 9. Measuring Point Distributions of Temperature and Deflection

For the loading process at room temperature, the deflection of specimen was increased with the load increment at the beginning stage. The first batch of concrete cracks at the corners was generated when applying the fourth level of the load, which was generally perpendicular to the slab diagonals, as shown in Figure 10(a). The maximum deflection of point DS2 was 19.5 mm.

When the loading process at room temperature was completed, the specimen was in a constant load for a period of time before the temperature rise.

The process of fire test on specimen TB-2 was as follows: (1) The time of temperature rise to 20 min, the temperature of furnace chamber was 726.7°C, and the temperatures for bottom and top of slab were 256.2°C and 30.5°C, respectively. The deflection of point DS2 was 31.7 mm. The width of first batch of concrete cracks was gradually increased, and the cracks were developed to the surrounding constraint concrete beams. (2) The time of temperature rise to 25 min, the second batch of concrete cracks at the corners was generated, as shown in Figure 10(b). The temperature of furnace chamber was 739.9°C, and the temperature for bottom and top of slab was 339.3°C and 35.3°C, respectively. The deflection of point DS2 was 35.3 mm. (3) The time of temperature rise to 43 min, a crack parallel to the long side of the slab was generated in the middle of long side, and a small amount of water vapor was appeared around the crack, as shown in Figure 10(c). The temperature of furnace chamber was 788.7°C, and the temperatures for bottom and top of slab were 576.5°C and 56.6°C, respectively. The deflection of point DS2 was 52.7 mm. (4) The time of temperature rise to 78 min, a group of cracks was ran through the slab, and the cracks in the corners became elliptical in shape. The temperature of furnace chamber was 893.7°C, and the temperatures for bottom and top of slab were 790.7°C and 75.7°C, respectively. The deflection of point DS2 was 96.2 mm. (5) The time of temperature rise to 90 min, the cracks were ran through in an elliptical shape on the top of slab, and the whole floor slab were elliptically went down.

After the fire test was completed, the overall deformation of specimen TB-2 was shown in Figures 11(a). The cracks on the bottom of slab and on the top of slab were shown in Figures 11(b) and (c), respectively. The following conclusions could be drawn. (1) There were more cracks in the long direction than in the short direction. (2) The tiny cracks were formed around the loading point because of the concentrated load. (3) The cracks on the top surface of slab were elliptically distributed.

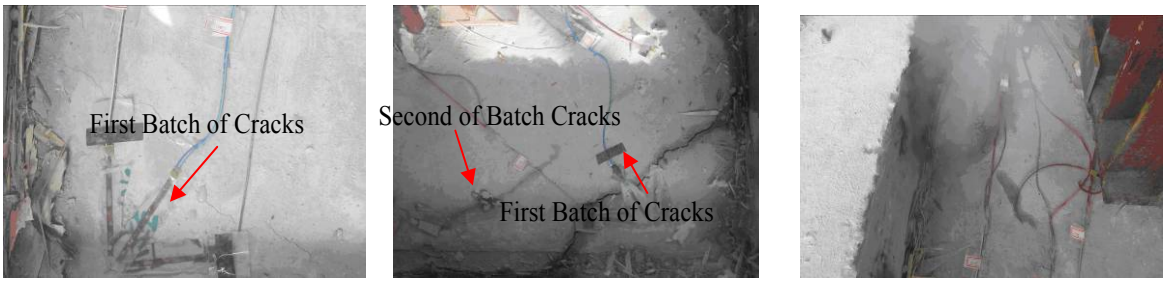

(a) First Batch of Crack (b) Second Batch of Cracks (c) Cracks in Long Direction

Figure 10. Development Processes of Cracks

(a) Overall Deformation (b) Cracks on bottom of Slab (c) Cracks on top of Slab

Figure 11. Failure Phenomenon

According to the failure phenomenon of fire test, when the deflection of slab in fire is very large, the compression reinforcement on the top of slab was gradually transformed into tensile reinforcement because of the restraint of the surrounding constraint concrete beams. The membrane action of composite floor was generated in the middle area (elliptical area). Conversely, a compression ring was formed outside the elliptical area, which was served as an anchor for reinforcement in the middle area. Thus, an elliptical crack was generated on the border of compression ring, due to the effect of tensile reinforcement.

3.6 Test Result

3.6.1 Temperature of furnace

The arrangement of the four temperature measuring points inside the fire furnace is shown in Figure 12(a). The temperature of furnace measured during the test process is shown in Figure 12(b) and (c). In the process of heating up, there was certain unevenness between the temperatures of each measuring point. The temperature at TP1 point was highest, and the temperature at TP4 point was lowest.

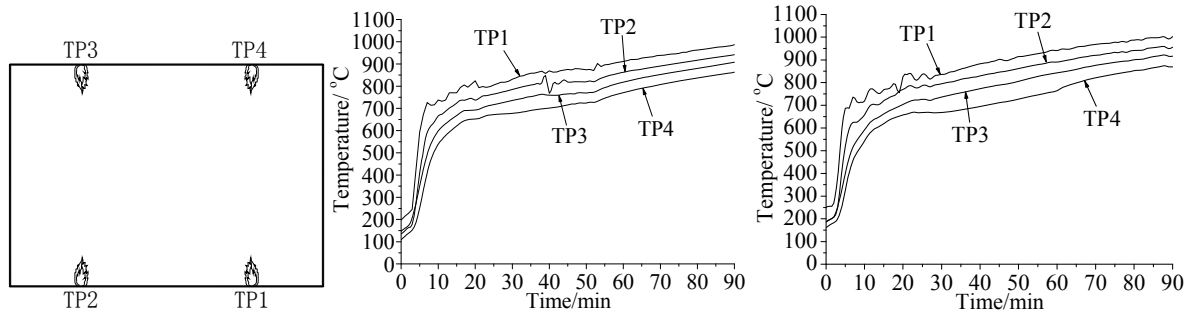

(a) Measuring points (b) Specimen TB-1 (c) Specimen TB-2

Figure 12. Furnace Temperatures in Fire

For the specimens TB-1 and TB-2 in fire, the contrasts of temperature curve between the furnace temperature and ISO-834 standard curve are shown in Figures 13(a) and (b), respectively. The difference value of temperature between the furnace temperature and ISO-834 standard curve is shown in the Figure 13(c). The following conclusions can be drawn from Figure 13. (1) The furnace temperature was lower than the temperature of ISO-834 standard curve. The trend of furnace temperature curve was consistent with the ISO-834 standard curve. (2) In the process of fire test, the difference value of furnace temperature was constant in 50-100°C. (3) In the initial stage of a fire, the heating rate of the furnace temperature was lower, and it was difficult to achieve the heating rate of ISO-834 curve. Thus, the maximum difference value of furnace temperature and temperature of IS0834 curve was approximately 250°C.

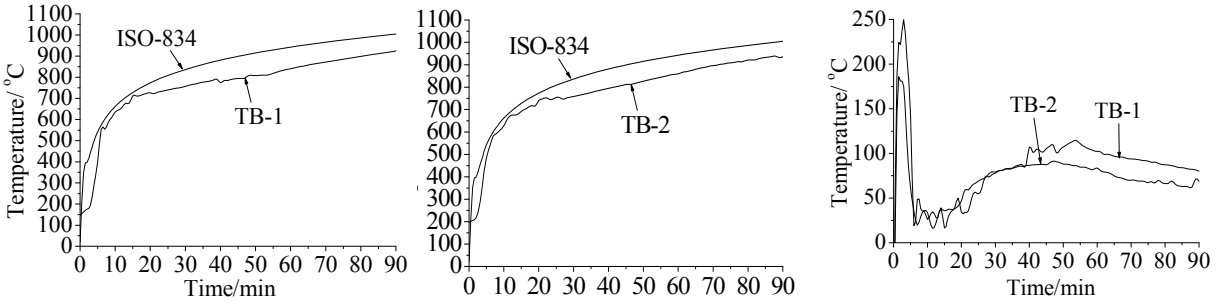

(a) Specimen TB-1 (b) Specimen TB-2 (c) Difference Value of Temperature

Figure 13. Comparisons between Furnace Temperature and Temperature of ISO-834 Curve

3.6.2 Temperature on the bottom of slab

The arrangement of temperature measuring point on the bottom of slab is shown in Figure 9(a). For the specimens TB-1 and TB-2, the comparisons of measuring point temperature with furnace temperature are shown in Figures 14(a) and (b), respectively. In the earlier stage (the time of temperature rise to 43 min), the temperature on the bottom of slab was slowly increased, and was apparently lower than the furnace temperature. When the temperature was reached to 100°C, it was constant for a period of time, because of the water vapor gathered around the thermocouple. In the later stage, the temperature on the bottom of slab was rapidly increased, and was gradually close to the furnace temperature.

3.6.3 Temperature on the top of slab

The arrangement of temperature measuring point on the top of slab is shown in Figure 9(b). For the specimens TB-1 and TB-2, the temperature curves of each measuring point are shown in Figures 15(a) and (b), respectively. The temperature on the top of slab was slowly increased, and was lower.

The highest temperature in the middle area on the top of slab was approximately 90.6°C, and the temperature in the corner area was approximately 64.8°C.

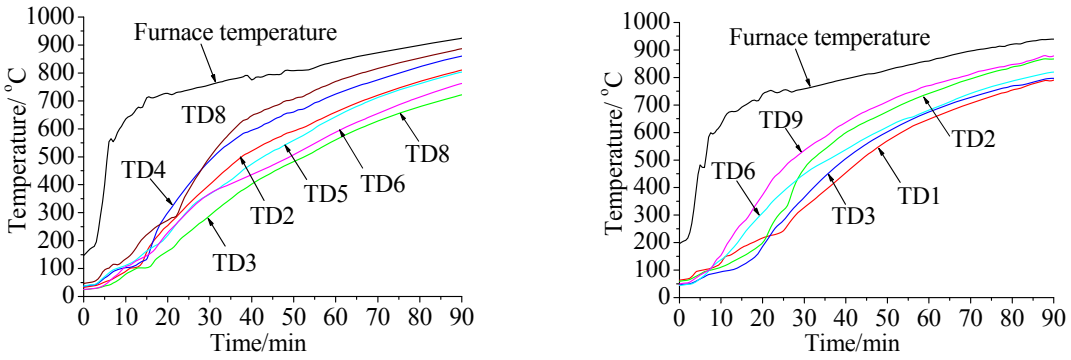

(a) Specimen TB-1 (b) Specimen TB-2

Figure 14. Comparisons between Temperature on the bottom of Slab and Furnace Temperature

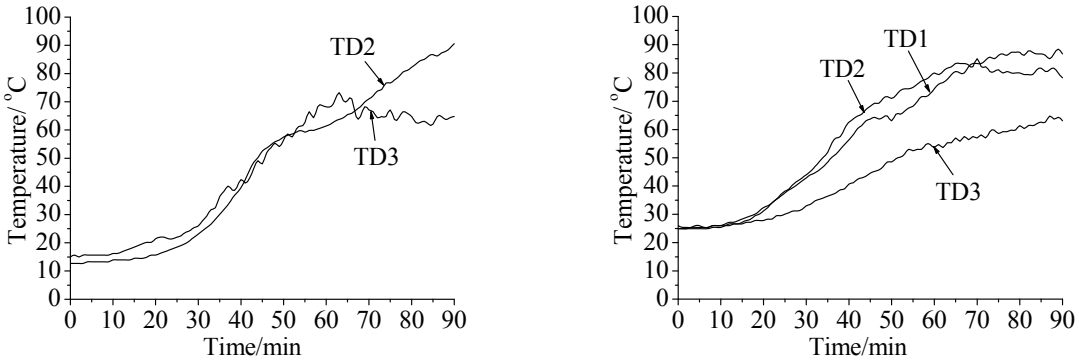

(a) Specimen TB-1 (b) Specimen TB-2

Figure 15. Temperature Curves on the Top of Slab

3.6.4 Temperature of Reinforcement

The arrangement of temperature measuring point for the reinforcement is shown in Figure 9(a). For the specimens TB-1 and TB-2, the temperature curves of reinforcements are shown in Figures 16(a) and (b), respectively. The temperature of reinforcement was gradually increased with the increment of fire time. However, the increased rate of temperature was slow, and the fluctuation was larger. The time of temperature rise to 30-40 min, a plateau was appeared in the temperature curve of reinforcement. The temperature of reinforcement was approximately 100°C, and was constant for 30 min, because a lot of water vapor was gathered around the reinforcement. In Figure 16, the temperature data of the part of measuring point (such as TS2, TS4 and TS7) were not collected, because of the thermocouples damaged.

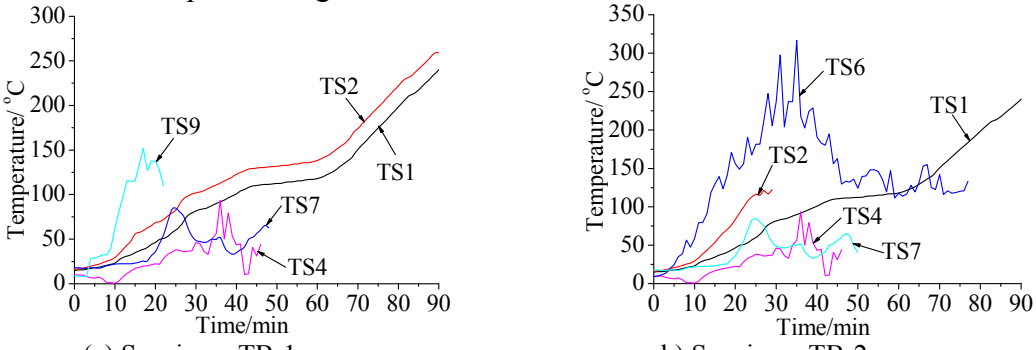

(a) Specimen TB-1 b) Specimen TB-2

Figure 16. Temperature of Reinforcement

3.6.5 Deflection of Slab

The arrangement of deflection measuring point is shown in Figure 9 (c). During the loading period at room temperature, the load-deflection curves of each measuring point on the specimens TB-1 and TB-2 are shown in Figure 17(a). The mid-span deflections of specimens TB-1 and TB-2 were 13.9 mm and 19.5 mm, respectively.

For the specimens TB-1 and TB-2 in fire, the deflection-time curves of each measuring point are shown in Figure 17(b). The deflection of slab was gradually increased with the increment of fire time. The deflection was slowly increased in the earlier stage, and was rapidly grown in the later stage. The time of temperature rise to 90 min, the mid-span deflections of specimens TB-1 and TB-2 were 92.6 mm and 94.9 mm, respectively. The two specimens were regarded as destroyed because all of the deflections were more than the limited value, which is L/20 (L represents the short span of the slab).

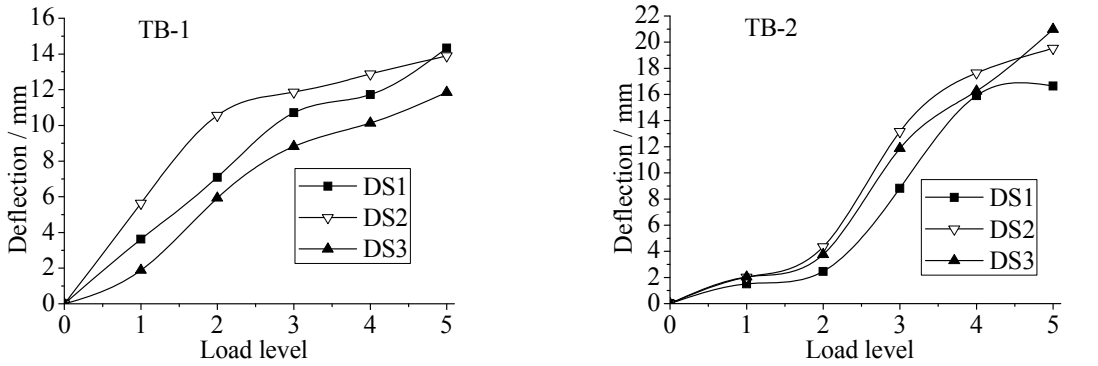

(a) Load-deflection Curves at Room Temperature

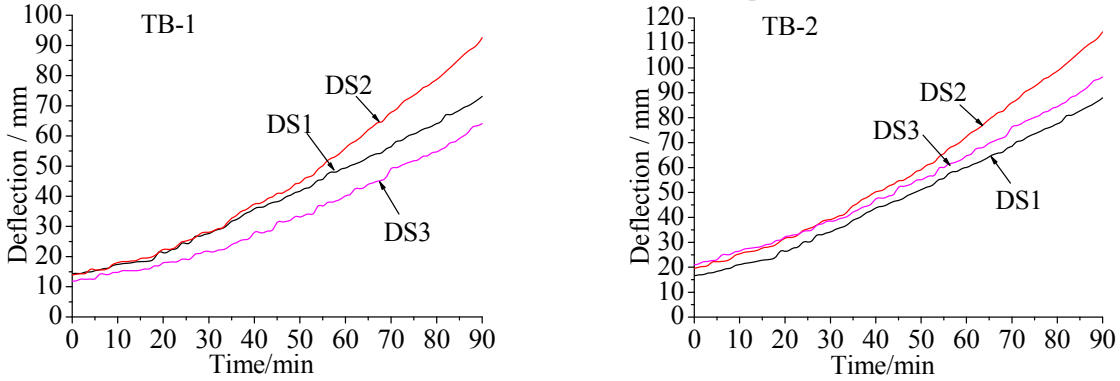

(b) Deflection-time Curves in fire

Figure 17. Deflection Curves of Slab

4. NUMERICAL SIMULATION OF TEMPERATURE FIELD IN FIRE

Based on the real curves of furnace temperature gained from the fire test, using the finite element software ABAQUS, a numerical simulation analysis of the 3-D transient temperature field was performed on the specimens TB-1 and TB-2 in the state of a single side under a fire. The internal temperature distribution of slab was studied. Compared with the test results, the accuracy of the finite element numerical simulation was verified. Furthermore, the relevant temperature data were provided to the later parametric analysis of a composite floor in fire.

4.1 Establishment of an Analytical Model

When performing the numerical simulation analysis of a 3-D transient temperature field on a composite floor in fire, the following basic assumptions should be made. (1) The furnace temperature is uniformly distributed. (2) The temperature distribution is not influenced by the deformation and stress state of a composite floor. (3) The thermal contact resistance between concrete and steel is neglected, and heat can be freely transferred. (4) The cracking and bursting of concrete have no influence on the temperature field.

According to the symmetry of the structure and loads, an analysis model to calculate the temperature field was established in a one-quarter size model of the real test specimen size. Different mesh designs were adopted on the concrete and profiled steel sheet. Sweep meshing was used to divide the elements of concrete, and free meshing was used to divide the elements of profiled steel sheet. To improve the boundary condition compatibility of the element meshes, the profiled steel sheet had the same element size as the concrete. The element meshes of concrete and profiled steel sheet are shown in Figures 18 (a) and 18 (b), respectively. The element mesh of reinforcement is shown in Figure 18 (c). The concrete element was in a Hex-dominated shape, and the profiled steel sheet element was in a Quad-dominated shape.

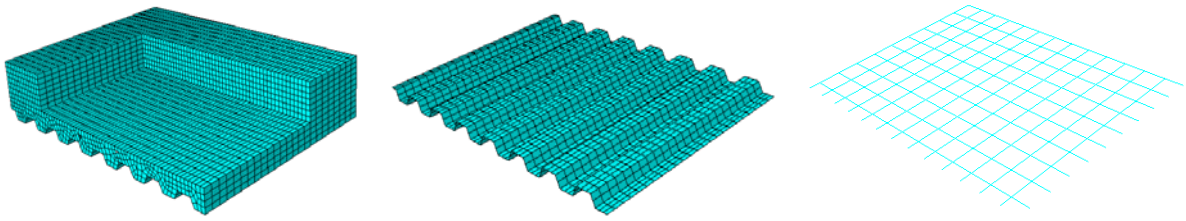

(a) Concrete (b) Profiled Steel Sheet (c) Reinforcement

Figure 18. Element Meshes of Slab

In the analytical model, the hexahedral solid element DC3D8 was adopted as the element of concrete, which transfers heat linearly with 8 nodes. The degree of freedom of the element node was the temperature scalar. The DS4 shell element was adopted as the element of profiled steel sheet. The heat-transferring truss element DC1D2 was used as the element of reinforcement.

4.2 Boundary Conditions and Relevant Parameters

The initial temperature T_0 of slab in the analytical model was 20°C. An adiabatic boundary was adopted in the central symmetrical boundary of slab, which made it easy to transfer heat between the different materials (concrete and steel). The degrees of freedom of the profiled steel sheet, concrete and reinforcement were bounded together.

The bottom slab of a composite floor was subjected to fire in the test. Heat was transferred between the bottom slab and furnace chamber through thermal convection and thermal radiation. According to the value of the parameters in the existing literature [10], the thermal convection coefficient α_c on the bottom surface of slab was $15\text{W/(m}\cdot{}^{\circ}\text{C)}$, and the radiation coefficient ε_r was 0.5. The thermal convection coefficient α_c on the top surface of slab was $5\text{W/(m}\cdot{}^{\circ}\text{C)}$, and the Stephen Boltzmann coefficient σ was $5.67\times10^{-8}\text{W/(m}^2\cdot\text{K}^4\text{)}$.

According to the test phenomenon in fire, the evaporation of water had a significant influence on the distribution of the temperature field in the composite floor. Therefore, the moisture content of composite floor was considered in the analysis model of finite element. The detail specific heat of concrete C_c was prescribed in the Eurocode4 [16]. (1) When the moisture content of concrete u=0, the specific heat C_c can be calculated by Eq. 2. (2) When the moisture content u is 0.15%, the specific heat C_c is $1470\,\mathrm{J/kg\cdot K}$ between 100°C to 115°C, and conforms to a linear relationship between 115°C and 120°C. The law in the other temperature is the same as that when u=0. (3) When the moisture content u is 3.0%, the specific heat C_c is $2020\,\mathrm{J/kg\cdot K}$ between 100°C and 115°C, and conforms to a linear relationship between 115°C and 120°C. The law in the other temperature is the same as that when u=0. (4) When the moisture content is 1.5%-3.0%, a linear interpolation is acceptable. The curves of specific heat with temperature for different moisture contents u are shown in Figure 19.

$$C_c = 900 + 80(\frac{T}{120}) - 4(\frac{T}{120})^2 \tag{2}$$

Where C_c represents the specific heat of concrete ($\mathrm{J/kg\cdot K}$) and T refers to the temperature of the concrete (K).

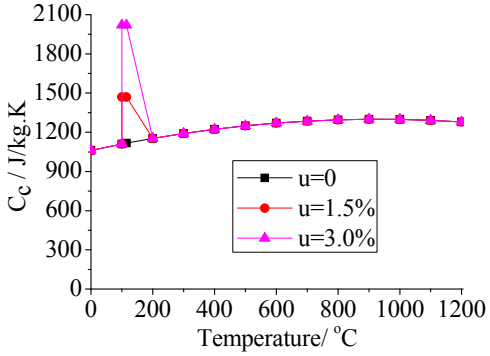

Figure 19. Curves of Specific Heat with Temperature

4.3 Comparisons between the Numerical Simulation Results and the Test Results

Through the numerical simulation analysis of temperature field, for specimen TB-1, the section temperature distribution of different moisture contents is shown in Figures 20 (a), (b) and (c). The following conclusions could be drawn from Figure 20. (1) The temperature was decreased step by step from the bottom to the top of slab. (2) The temperature at the crest of the profiled steel sheet was increased the fastest. The temperature on the two sides was higher than that in the middle at the crest of the profiled steel sheet, and the temperature in the middle was higher than that on the two sides at the trough of the profiled steel sheet. (3) The temperature on the top surface of slab was mainly distributed uniformly and was much lower than the temperature on the bottom surface of slab. Comparing the temperature profile of the different moisture contents of concrete, it could be concluded that the higher the moisture content is, the lower the section temperature is. Furthermore, the moisture content has a smaller influence on the temperature of the bottom slab than that of the top slab.

The comparisons of temperature between numerical simulation results and test results for the specimens TB-1 and TB-2 are shown in Figure 21 and Figure 22, respectively. The results for part of measuring points were provided in the figures.

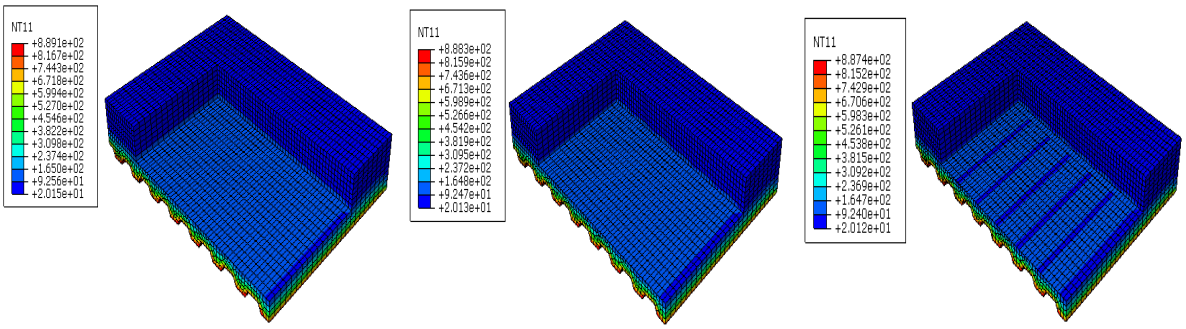

(a) u=0 (b) u=0.15% (c) u=3.0%

Figure 20. Temperature Distribution of Different Moisture Content

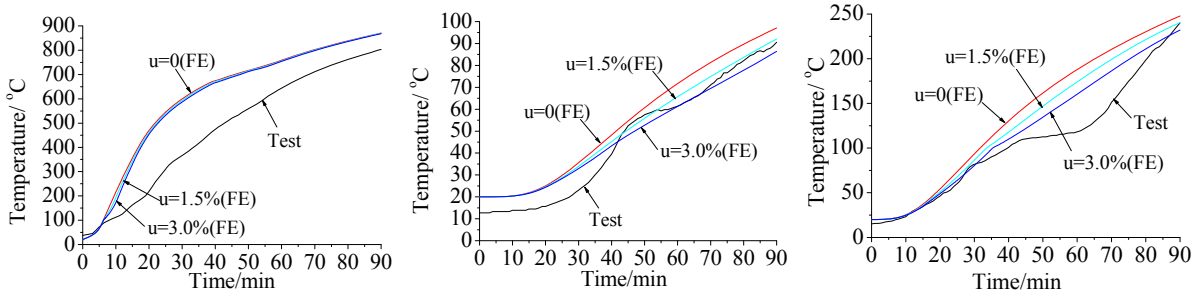

(a) Point TD5 on the bottom of Slab (b) Point TU2 on the top of Slab (c) Point TS1 of Reinforcement

Figure 21. Comparison of Temperature between the Numerical Simulation Results and Test Results for Specimen TB-1

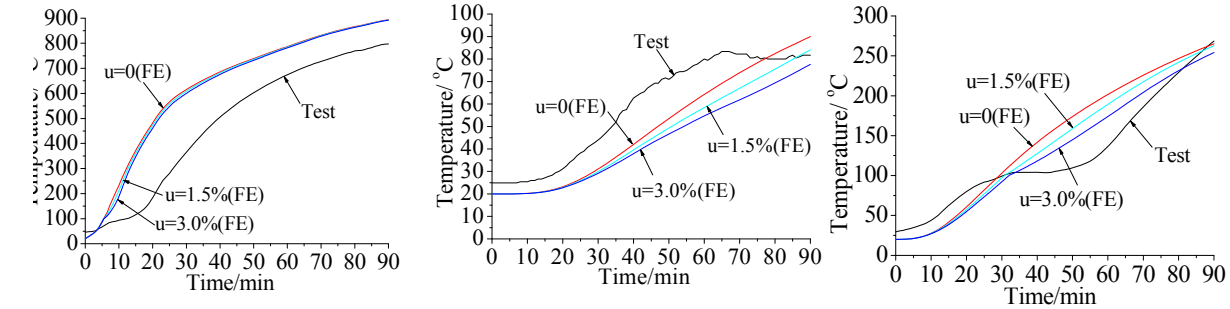

(a) Point TD3 on the bottom of Slab (b) Point TU2 on top of Slab (c) Point TS3 of Reinforcement

Figure 22. Comparison of Temperature between the Numerical Simulation Results and Test Results for Specimen TB-2

As shown in Figure 21 and Figure 22, the moisture content of concrete has a different influence on the temperatures at the areas of slab in the fire. The influence on the high temperature area (the bottom slab) was not obvious, and the influence on the low temperature area (the top slab and reinforcement) was more obvious. The difference value between the numerical simulation results and the test result was large in the early period of fire test, and the difference value was gradually decreased with the increment of temperature. The main causes were analyzed. (1) The initial temperature in the numerical simulation model was 20°C. However, the initial temperature of furnace in the fire test was set at a high value to simulate the ISO-834 standard curve. (2) In the process of fire test, a platform was appeared in the temperature curve of slab because of water evaporation in the concrete. Though the specific heat C_c between 100°C to 200°C was reduced in the finite element model and the final result was revised, the platform in the temperature curve was still hard to simulate accurately. (3) The discreteness of concrete material was larger, and is difficult to simulation.

Based on the above analysis, for the temperature field of a composite floor in fire, the simulation result was generally in agreement with the test result. When the moisture content of concrete was 1.5%, the simulation results were the most consistent with the test results. Thus, it is suggested that the moisture content of concrete be set to 1.5% in the analysis of temperature field for a composite floor in fire.

5. PARAMETRIC ANALYSIS ON MEMBRANE ACTION OF A COMPOSITE FLOOR IN FIRE

5.1 Establishment of the Structural Analysis Model

To simplify the structural analysis, the following assumptions should be made when establishing finite element model of a composite floor in fire. (1) The creep of concrete and steel at a high temperature was ignored. (2) The slip between the different materials (concrete and steel) was ignored. (3) The distribution of temperature field for a composite floor in fire is not influenced by the stress state.

The structural analysis model was established by the finite element software ABAQUS, with the sequentially coupled thermal-stress analysis method as the computation method. The computing element was divided by the same method as the numerical simulation model of temperature field. Because the membrane action of a composite floor in fire was mainly studied in the structure analysis, the ultimate deformation was larger when the floor was damaged, which may lead to distortion in the computing element. Therefore, a 3-D solid element in a reduced integration format with 8 nodes (C3D8R) was adopted as the element of concrete. The reinforcement was simulated by a 2-node truss element (T3D2), and the profiled steel sheet was simulated by a 4-node shell element (S4R) in a reduced integration format. According to the symmetry principle, the size of structural analysis model for a composite floor in fire was a quarter of the actual size. The mesh element of structural analysis model was shown in Figure 23 (a).

The boundary conditions and contact boundaries in the structural analysis model were set up in the following ways. (1) The symmetrical boundary perpendicular to the X axis were fixed on the constraint condition ($U_1=U_{R2}=U_{R3}=0$), which was the same as the boundary perpendicular to the Y axis ($U_2=U_{R2}=U_{R3}=0$). The slab was supposed to be simply supported. The boundary constraints in the X direction were $U_1=U_3=U_{R2}=U_{R3}=0$, and the boundary constraints in the Y direction were $U_2=U_3=U_{R1}=U_{R3}=0$, as shown in Figure 23 (b). (2) The degrees of freedom of the profiled steel sheet, concrete and reinforcement were bounded together. The degree of freedoms between the profiled steel sheet and concrete were tied by the constraint. The main surface was on the concrete, and the dependent surface was on the profiled steel sheet, as shown in Figure 23 (c). An embedded constraint was adopted as the constraint between the reinforcement and concrete.

5.2 Verification of the Structural Analysis Model

The analysis results of the finite element model were compared with the test results, and the deflection comparisons of specimen TB-1 and TB-2 are shown in Figures 24 (a) and (b), respectively.

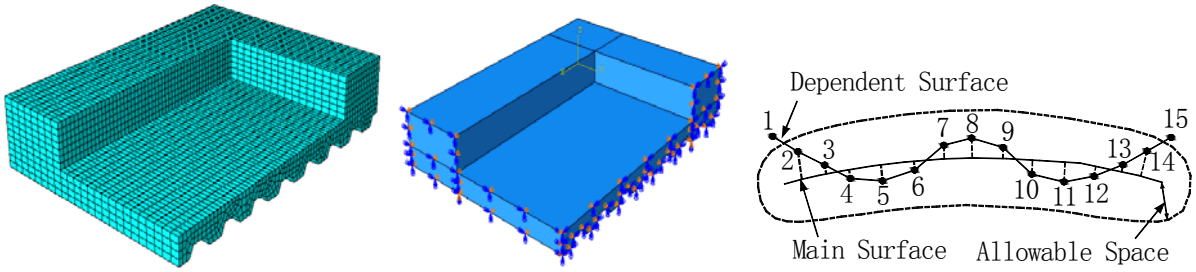

(a) Element Mesh (b) Boundary Condition (c) Contact Boundary

Figure 23. Structural Analysis Model of a Composite Floor in Fire

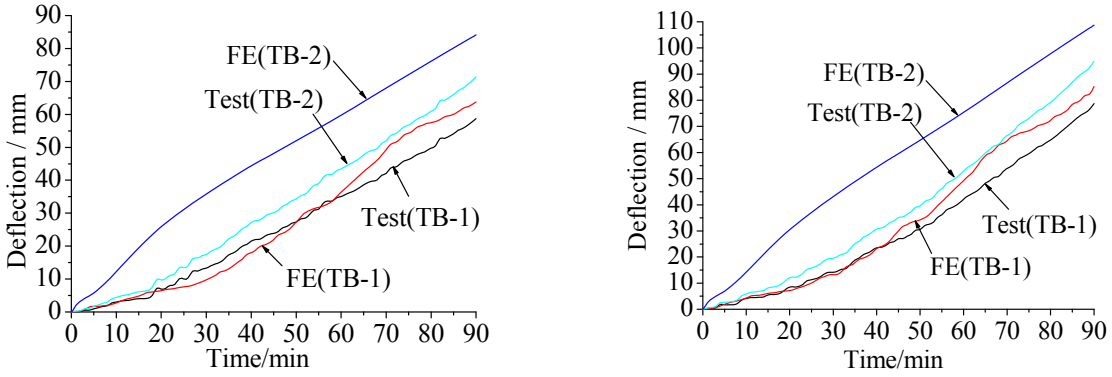

(a) Point DS1 (b) Point DS2

Figure 24. Comparisons of Analysis Results and Test Results for the Deflection of Slab

According to Figures 24 (a) and (b), for specimen TB-1, the analysis results of the deflection were basically in consistent with the test results, though the analysis results were slightly larger than test results in the late period of fire. For specimen TB-2, the trends of deflection curve between the analysis results and the test results were the same, but there was a large difference of deflection values between the two in the early period of fire. With the increment of temperature, the difference was reduced gradually.

By the comparison of deflection between the analysis results and the test results, the structural analysis model of a composite floor adopted in this paper is feasible, and the analytical result is reliable.

5.3 Parametric Analysis

The ultimate bearing capacity of a composite floor with the membrane action considered is related to many factors, such as length-to-width ratio L/B (L refers to the size of long side, B refers to the size of short side), thickness of concrete cover c, concrete strength f_c, yield strength of reinforcement f_y, reinforcement ratio ρ_s and thickness of slab h. Based on the structural analysis model of a composite floor in fire, the parametric analysis was carried out to investigate the influence factors on the membrane action of slab in fire.

The basic parameters in the finite element model were set as follows. The length of slab L was 3.0m and the width B was 3.0m. A profiled steel sheet of YX51-253-760 was adopted, with a thickness of 1 mm, and the yield strength f_y was 235 N/mm^2. The diameter of reinforcement was 6mm, and the yield strength f_y was 310 N/mm^2. The reinforcement ratio ρ_s was adjusted by changing the interval distance of the reinforcements. The thickness of concrete cover c was 25mm. The strength of concrete f_c was 20.1N/mm^2. The thickness of slab h was 130mm. The fire duration time of slab was 90 min.

The increasing coefficient *e* of bearing capacity in fire can be calculated by Eq. 3, which the membrane action of a composite floor was considered.

$$e = \frac{q_T}{q_0} \tag{3}$$

Where q_T represents the ultimate bearing capacity of a composite floor that the membrane action is not considered at T °C, and q_0 refers to the ultimate bearing capacity of a composite floor that the membrane action is considered at room temperature.

5.3.1 Length-to-width L/B

The influence of length-to-width ratio *L*/*B* on the membrane action of a composite floor in fire was researched by changing the length and width of slab, if the other parameters were constant. The length-to-width ratio *L*/*B* of slab was respectively selected as 1.0, 1.5, 2.0, 2.5, 3.0 or 3.5, and the corresponding finite element model of structural analysis was established. The ultimate bearing capacities of a composite floor at high temperature were calculated. At the same time, for contrastive analysis, the ultimate bearing capacities were worked out according to the method proposed by Zhang et al. [8]. The increasing coefficient curves of bearing capacity with the length-to-width ratio *L*/*B*, which were calculated by different methods, are shown in Figure 25.

By the figure 25, we can see that (1) the results of finite element analysis have a similar trend with the computational results by Zhang. However, the finite element results are always lower than the results by Zhang. (2) The larger the length-to-width *L*/*B* is, the smaller the increasing coefficient of bearing capacity *e* is. For a composite floor with the lager length-to-width ratio in fire, the reinforcements along the short span were early yield, and the reinforcements along the long span were not fully used. Therefore, it is suggested that the length-to-width ratio of a composite floor should be smaller than 2.0 in the fire-resistant design if the membrane action of slab is considered.

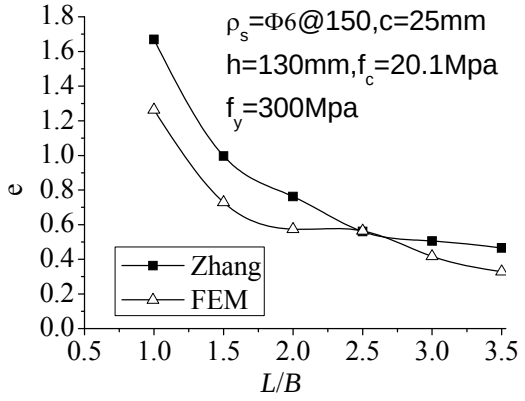

Figure 25. Increasing Coefficient of Bearing Capacity with Length-to-Width

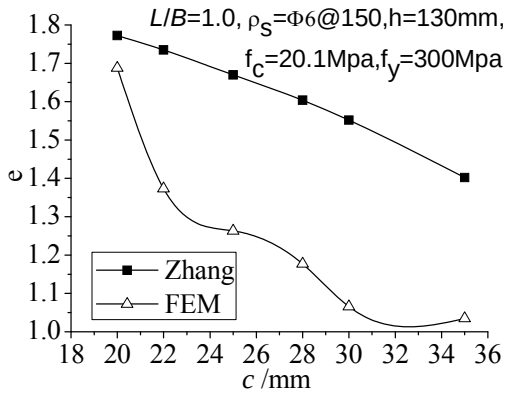

Figure 26. Increasing Coefficient of Bearing Capacity with Thickness of Concrete Cover

5.3.2 Thickness of concrete cover c

If the other parameters were constant, the thickness of concrete cover *c* was respectively selected as 20, 22, 25, 28, 30 or 35 mm, and the corresponding finite element model of structural analysis was established. The ultimate bearing capacities of a composite floor at high temperature were determined. At the same time, for contrastive analysis, the ultimate bearing capacities were calculated according to the method proposed by Zhang et al. [8].The increasing coefficient curves

of bearing capacity with the thickness of concrete cover *c*, which were calculated by different methods, are shown in Figure 26.

By the figure 26, we can see that (1) the results of finite element analysis are always lower than the results by Zhang. (2) The larger the thickness of concrete cover *c* is, the smaller the increasing coefficient of bearing capacity *e* is. The high thickness of concrete cover leads to an increment of temperature in the reinforcement, to the disadvantage of the generation of membrane action in fire. Thus, the concrete cover should not be thick in fire-resistant design.

5.3.3 Strength of Concrete f_c

If the other parameters were constant, the strength of concrete f_c was respectively selected as 13.4, 16.7 or 20.1 N/mm^2, and the corresponding finite element model of structural analysis was established. The ultimate bearing capacities of a composite floor at high temperature were calculated. At the same time, for contrastive analysis, the ultimate bearing capacities were worked out according to the method proposed by Zhang et al. [8].The increasing coefficient curves of bearing capacity with the strength of concrete f_c, which were calculated by different methods, are shown in Figure 27.

By the figure 27, we can see that the strength of concrete f_c has a small influence on the increasing coefficient of bearing capacity *e*. The strength of concrete does not greatly influence on the membrane action of a composite floor in fire, and the membrane force is mainly provided by the reinforcements.

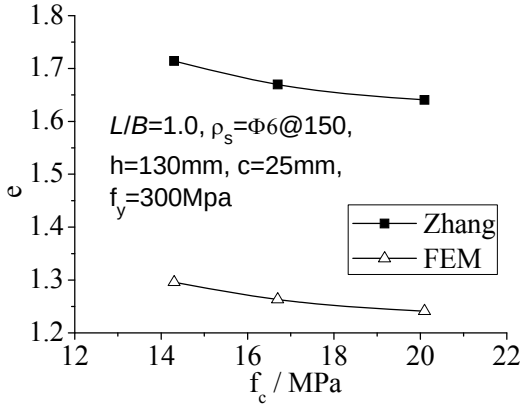

Figure 27. Increasing Coefficient of Bearing Capacity with Strength of Concrete

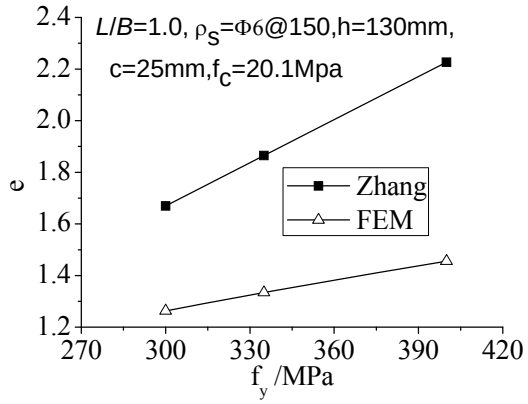

Figure 28. Increasing Coefficient of Bearing Capacity with Strength of Reinforcement

5.3.4 Strength of Reinforcement f_y

If the other parameters were constant, the strength of reinforcement f_y was respectively selected as 300, 335 or 400 N/mm^2, and the corresponding finite element model of structural analysis was established. The ultimate bearing capacities of a composite floor at high temperature were calculated. At the same time, for contrastive analysis, the ultimate bearing capacities were worked out according to the method proposed by Zhang et al. [8].The increasing coefficient curves of bearing capacity with the strength of reinforcement f_y, which were calculated by different methods, are shown in Figure 28.

By the figure 28, we can see that the stronger the strength of reinforcement is, the larger the increasing coefficient of bearing capacity *e* is. The strength of reinforcement is the main influence factor on the membrane action a composite floor in fire.

5.3.5 Reinforcement ratio ρ_s

If the other parameters were constant, the reinforcement ratio ρ_s was adjusted only by changing the interval distance of reinforcement d_s. The interval distances of reinforcement d_s were respectively selected as 100, 130, 150, 180, 200 or 230 mm, and the corresponding finite element model of structural analysis was established. The ultimate bearing capacities of a composite floor at high temperature were calculated. At the same time, for contrastive analysis, the ultimate bearing capacities were worked out according to the method proposed by Zhang et al. [8].The increasing coefficient curves of bearing capacity with the interval distance of reinforcement d_s (the reinforcement ratio ρ_s), which were calculated by different methods, are shown in Figure 29.

By the figure 29, we can see that the increasing coefficient of bearing capacity *e* has a decreasing trend as the interval distance of reinforcement d_s increases. The reinforcement ratio is also the main influence factor on the membrane action a composite floor in fire.

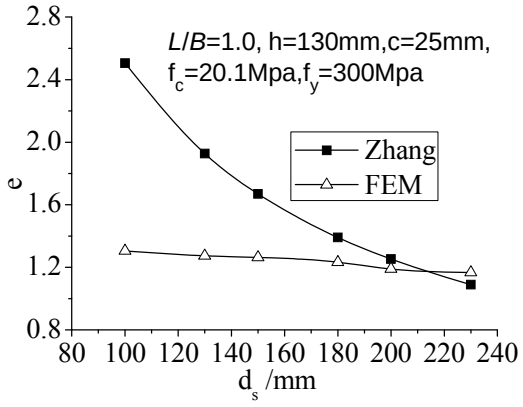

Figure 29. Increasing Coefficient of Bearing Capacity with Reinforcement Ratio

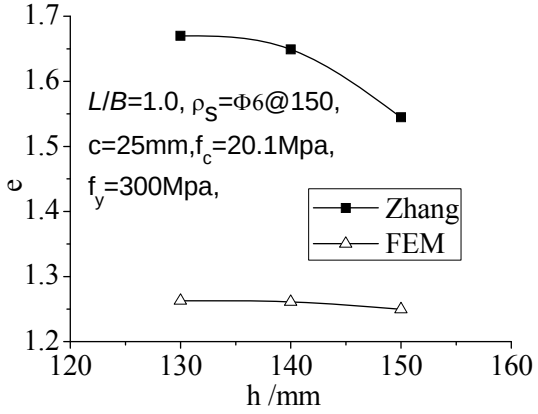

Figure 30. Increasing Coefficient of Bearing Capacity with Thickness of Slab

5.3.6 Thickness of slab h

If the other parameters were constant, the thickness of slab *h* was respectively selected as 130, 140 or 150 mm, and the corresponding finite element model of structural analysis was established. The ultimate bearing capacities of a composite floor at high temperature were determined. At the same time, for contrastive analysis, the ultimate bearing capacities were calculated according to the method proposed by Zhang et al. [8].The increasing coefficient curves of bearing capacity with the thickness of slab *h*, which were calculated by different methods, are shown in Figure 30.

By the figure 30, we can see that the thickness of slab *h* has a small influence on the increasing coefficient of bearing capacity *e*. The thickness of slab does not greatly influence on the membrane action of a composite floor in fire.

6. CONCLUSIONS

By the research and analysis mentioned above, the following conclusions can be drawn.

(1) The experimental phenomenon demonstrates that the composite floor remained integrated and is not burn-through, from the beginning to the end of the fire test, which could provide an important safeguard to avoid integral collapse. Slip between the steel sheet and concrete is also found in the

fire test. It is suggested that shear connectors be installed between the two in the subsequent fire resistance research of a composite floor.

(2) According to the specimens tested in fire, the shape of cracks distribution on the top surface of the composite floor was an ellipse. Almost all of the reinforcements in the slab were in a state of tension. The central area of the composite floor was slide down in an ellipse shape with a large deformation, which the membrane action of a composite floor in fire was verified. The formation mechanism of membrane action for a composite floor in fire was revealed. Finally, the judgment criterion on the formation of membrane action in fire test was provided.

(3) A numerical simulation analysis for the temperature field of a composite floor in fire was performed through the finite element software ABAQUS. The simulation results were compared with the test results, and the feasibility and accuracy of analytical method was verified. Furthermore, the analytical results of temperature field demonstrated that the moisture content of concrete had little influence on the high-temperature area of slab, and larger influence on the low-temperature area of slab. It was suggested that the moisture content of concrete u be 1.5% in the fire resistance analysis of a composite floor.

(4) A parametric analysis was performed to investigate the main influence factors on the membrane action of a composite floor in fire. The analytical result demonstrates that the length-to-width L/B is the main influence factor on the membrane action of a composite floor in fire, and it is suggested that the length-to-width L/B be less than 2.0 to make full use of the membrane action of a composite floor. The thickness of concrete cover c, the thickness of slab h and the strength of concrete f_c had little influence on the membrane action. The strength of reinforcement f_y and the reinforcement ratio ρ_s are beneficial for improving the bearing capacity of a composite floor in fire.

ACKNOWLEDGEMENTS

The authors gratefully acknowledge the financial support of the National Natural Science Foundation of China (No. 51378105). The research was also supported by the Priority Academic Program Development of Jiangsu Higher Education Institutions and Jiangsu Provincial Forward-Looking Cooperation Foundation of Industry, Education and Research (No. BY2012200). These financial supports are gratefully acknowledged.

REFERENCES

[1] Chen, Y.O., Cheng, M.K. and Liu, J.K., “Experimental Research on Fire-resistance of Metal Deck Composite floor”, Industrial Construction, 1999, Vol. 29, No. 12, pp. 23−27.

[2] Li, G.Q., Yin, Y.Z. and Jiang, S.C., “Analysis of the Temperature Distribution in Composite Slabs Subjected to Fires”, Journal of Building Structure, 1998, Vol. 19, No. 5, pp. 47−50.

[3] Lim, L., Buchanan, A. and Moss, P., et al., “Numerical Modeling of Two-way Reinforced Concrete Slabs in Fire”, Engineering Structures, 2004, Vol. 26, No. 8, pp. 1081−1091.

[4] Bailey, C.G., White, D.S. and Moore, D.B., “The Tensile Membrane Action of Unrestrained Composite Slabs Simulated under Fire Conditions”, Engineering Structures, 2000, Vol. 22, pp. 1583−1595.

[5] Chen, L.G., Dong, J.L. and Dong, Y.L., “Analysis on the Deformation of the Reinforced Concrete Slabs under Fire”, Journal of Qingdao Institute of Architecture and Engineering, 2005, Vol. 26, No. 3, pp. 1−4.

[6] Li, G.Q., Zhou, H.S. and Guo, S.X., "Mechanism and Theoretical Model Membrane Action in Slabs of Steel Buildings Subjected to Fire", Journal of Building Structures, 2007, Vol. 28, No. 5, pp. 40−47.
[7] Zhang, N.S. and Li, G.Q., "An Innovative Analytical Method for the Membrane Action of Composite floors in Fire", China Civil Engineering Journal, 2009, Vol. 42, No. 3, pp. 29−35.
[8] Li, G.Q. and Zhang, N.S., "Experimental Study of Membrane Action of Composite floors under Fire", China Civil Engineering Journal, 2010, Vol. 43, No. 3, pp. 24−31.
[9] Li, G.Q., Guo, S.X. and Zhou, H.S., "Model Validation and Application of Membrane Action in Slabs of Steel Buildings Subjected to Fire", Journal of Building Structures, 2007, Vol. 28, No. 5, pp. 48−53.
[10] Lamont, S., Usmani, A.S. and Drysdale, D.D., "Heat Transfer Analysis of the Composite Slab in the Cardington Frame Fire Tests", Fire Safety Journal, 2001, Vol. 36, pp. 815−839.
[11] Gillie, M., Usmani, A.S. and Rotter, J.M., "A Structural Analysis of the Cardington British Steel Comer Test", Journal of Constructional Steel Research, 2002, Vol. 58, pp. 427−442.
[12] Usmani, A.S. and Cameron, N.J.K., "Limit Capacity of Laterally Restrained Reinforced Concrete Floor Slabs in Fire", Cement & Concrete Composites, 2004, Vol. 26, pp. 127−140.
[13] Bailey, C.G. and Moore, D.B., "The Structural Behaviour of Steel Frames with Composite floors Subject to Fire: Part1: Theory", The Structural Engineer, 2000, Vol. 78, No. 11, pp. 19−27.
[14] Bailey, C.G. and Moore, D.B., "The Structural Behaviour of Steel Frames with Composite floors Subject to Fire: Part2: Design", The Structural Engineer, 2000, Vol. 78, No.11, pp. 28−33.
[15] Bailey, C.G., "Efficient Arrangement of Reinforcement for Membrane Behaviour of Composite floors in Fire Conditions", Journal of Constructional Steel Research, 2003, Vol. 59, pp. 931−949.
[16] EC2, "Euro code 2: Design of Concrete Structures, Part 1-2: General Rules — Structural Fire Design", European Committee for Standardization, ENV 1993-1-2, CEN, Brussels, 1992.